AD-A041 218 BELL AEROSPACE TEXTRON BUFFALO N Y F/G 11/6
CATHODIC KINETICS DURING CORROSION OF 5456-H117 ALUMINUM ALLOY --ETC(U)
1977 J A DAVIS , G A GEHRING, A A WATTS N00014-75-C-1087
UNCLASSIFIED NL

1 OF 1
AD
A041218

END
DATE
FILMED
7-77

CATHODIC KINETICS DURING CORROSION OF 5456-H117 ALUMINUM ALLOY BY HIGH VELOCITY SEA WATER

J.A. Davis
Allegheny Ludlum Steel Corporation
Research Center
Brackenridge, Pennsylvania 15014

G.A. Gehring, Jr.
Ocean City Research Corporation
Beach Thorofare and Tennessee Ave.
Ocean City, New Jersey 08226

A.A. Watts
Bell Aerospace Textron
P.O. Box One
Buffalo, New York 14240

Paper Prepared
for Submittal to
The 7th International Congress
on Metallic Corrosion
Rio de Janeiro, P. J., Brazil

October 1978

Contract No. N00014-75-C-1087

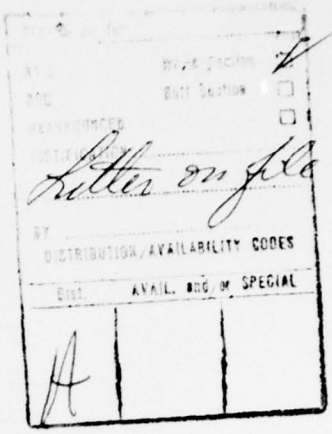

CATHODIC KINETICS DURING CORROSION OF 5456-H117 ALUMINUM ALLOY BY HIGH VELOCITY SEA WATER

J.A. Davis
Allegheny Ludlum Steel Corporation
Research Center
Brackenridge, Pennsylvania 15014

G.A. Gehring, Jr.
Ocean City Research Corporation
Beach Thorofare and Tennessee Ave.
Ocean City, New Jersey 08226

A.A. Watts
Bell Aerospace Textron
P.O. Box One
Buffalo, New York 14240

Davis, Watts and Gehring [1] examined the pitting behavior of 5456-H117 and 1100 aluminum alloys over a sea water velocity range of zero to 60 knots (zero to 31 m/s). They observed that the critical pitting potential, protection potential and corrosion potential, shifted in the active direction as the sea water velocity was increased. These potentials undergo a discontinuous noble shift in the velocity range of 15 to 30 knots (7.7 to 15.4 m/s) depending on specimen geometry. This discontinuous shift was explained on the basis of either a transition from laminar to turbulent flow or the onset of cavitation. These authors observed pitting corrosion with constant applied potential at all velocities and at potentials more active than the critical pitting potential. The extent of pitting decreased as the velocity increased and as the applied potential became more active.

Pryor [2] and Galvele [3] had previously proposed that valid critical pitting potentials can be determined on aluminum alloys exposed to deaerated sodium chloride solutions, but that pitting potentials determined in oxygen containing chloride environments do not correspond with potentials required to initiate pitting. Wood et al [4] have proposed that the morphology and mechanisms of pitting are different for pits initiated at potentials more noble than the critical pitting potential when compared to pits formed at potentials more active than the critical pitting potential. Macropits and micropits are observed at the more noble potentials while only micropits are observed at the more active potentials.

Hartt [5] observed a steady state and a non-steady state pitting potential for aluminum alloys exposed to quiescent sea water with the steady state value of 40 mV more active than the non-steady state value. The non-steady state values were determined potentiodynamically while the steady state values were determined using long term exposure tests. Groover, Lennox and Peterson, [6] Alior, [7] and Fink and Boyd [8] have reported that aluminum alloys will pit in sea water if their corrosion potentials are more noble than -0.9 V_{SCE} for alloys having pitting potentials of about -0.7 V_{SCE}. Hartt [5] attributed pitting in the potential range of -0.7 to -0.9 V_{SCE} to the presence of ferric and cupric ions in the sea water that cause local film breakdown in the potential region between the critical pitting potential and -0.9 V_{SCE}.

Franz and Novak [9] have determined critical pitting potentials for 99.99 percent pure aluminum exposed to 0.1 N sodium chloride using a rotating disk electrode. They observed a noble shift in critical pitting potential by 25 to 30 mV as the rotational velocity was increased to 2000 rpm (about 5 knots or 2.1 m/s). The noble shift in critical pitting potential was explained on the basis that increasing velocity decreases the boundary layer thickness and the local hydrogen ion concentration is reduced. More noble potentials are required to initiate pitting with the reduced hydrogen ion concentration.

Danek [10] examined the influence of sea water velocity on pitting of aluminum alloys over a velocity range of zero to 70 knots (zero to 36.0 m/s) using a water jet test facility. Danek reported that pitting did not occur above a critical velocity of 30 knots (15.4 m/s) under freely corroding conditions based on visual observations. Danek proposed that the limiting oxygen diffusion current density increased as the velocity increased and that the increased oxygen supply inhibited the pitting reaction.

Several recent studies of the influence of velocity on the corrosion behavior of marine materials have included considerations of hydrodynamics and mass transfer on corrosion behavior. [1, 11 to 14] These studies have shown that limiting oxygen diffusion currents should be proportional to velocity to the one-half power with laminar flow and velocity to the one-fifth power under turbulent flow conditions.

The purpose of this investigation was to measure limiting oxygen diffusion current densities as a function of velocity, to study cathodic kinetics on 5456-H117 aluminum alloy as a function of velocity and to conduct constant potential tests at more active potentials than -0.9 V_{SCE}. The limiting oxygen diffusion current density was measured using a platinum clad tantalum electrode exposed

to sea water velocities of zero to 60 knots (zero to 31 m/s). Cathodic kinetics were examined by recording cathodic polarization curves on 5456-H117 aluminum alloy over the same velocity range. Constant potential tests were conducted at selected velocities at potentials more active than -0.9 $V_{(SCE)}$ to determine if pitting could be suppressed at the more active potentials. Finally, a model was proposed to explain the observations from this and previous studies.

EXPERIMENTAL

Materials

The materials for this study were 5456-H117 aluminum alloy and platinum clad tantalum. The 5456-H117 aluminum alloy typically has a composition range of 4.7 to 5.5 percent magnesium, 0.5 to 1.0 percent manganese and 0.05 to 0.20 percent chromium. The H-117 temper was developed to minimize the occurrence of exfoliation during exposure to sea water. The platinum clad tantalum consists of a thin sheet of platinum roll bonded to tantalum. The platinum provides the current efficiency and the tantalum provides strength and a high breakdown potential in sea water.

Test Electrolyte

Fresh, unpolluted sea water was used for all experiments. The sea water is drawn from the inlet bay in Ocean City, New Jersey, filtered through sand and diatomaceous earth to remove silt and sand, and controlled to a temperature of 75 ± 5°F (23.9 ± 2.8°C) to minimize the influence of seasonal temperature variations on the results. The sea water typically contained 7 ppm oxygen, the pH remained at 8.2 and the salinity ranged from 29 to 36 ppt.

Test Facility

Tests in quiescent sea water were conducted in a 55-gallon non-metallic container. The sea water was completely replenished once an hour for the duration of the tests.

The test facility for obtaining velocities from 5 to 90 knots is a high speed water wheel shown schematically in Figure 1. Velocities are developed by rotation of an open cylindrical container in a horizontal plane about a vertical shaft. The radius of the wheel is 31 inches and the available test area is a toroid of water six inches deep and 18 inches high. Specimens are positioned three inches from the outer wall, where a velocity of 90 knots is generated at 650 rpm.

Electrochemical Instrumentation

Limiting oxygen diffusion current densities and cathodic polarization curves were established potentiodynamically with potentials recorded on the silver/silver chloride scale using a

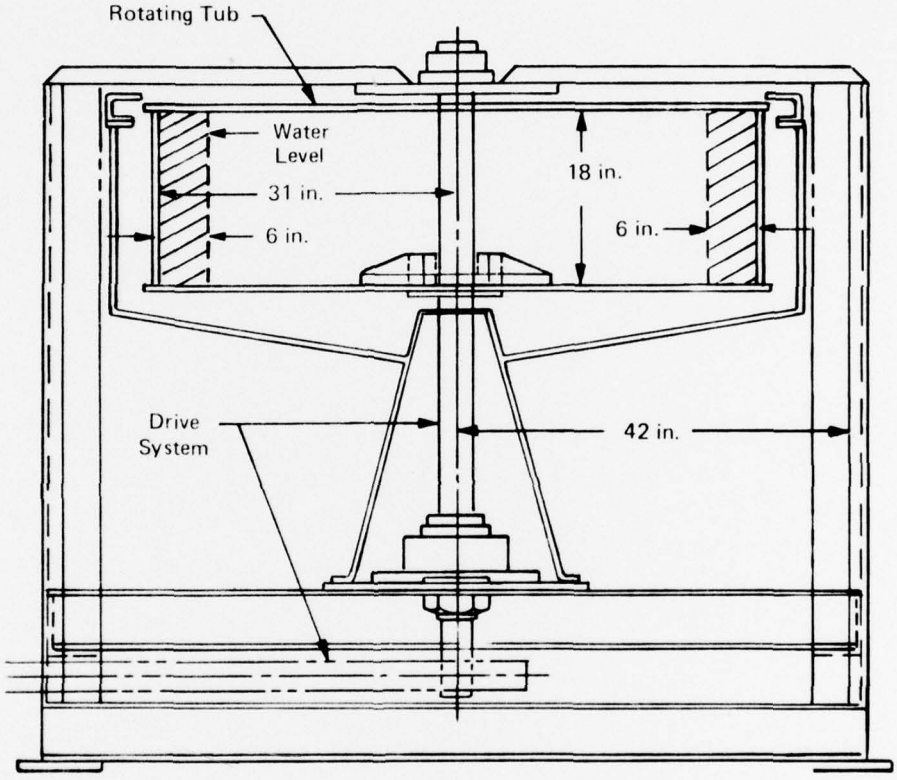

Figure 1. High Speed Water Wheel

high input impedance electrometer and currents were recorded using a series of precision resistors in the counter electrode circuit. The precision resistors were selected to give current ranges of 0-1 μ A to 0-1 A. Constant potential tests were conducted potentiostatically.

Specimen Design

Limiting oxygen diffusion current densities were determined using a platinum clad tantalum specimen, a plexiglass specimen holder, and a nylon coated steel strut as shown schematically in Figure 2. Electrical contact to the specimen was achieved using the steel supporting strut as an electrical lead.

The 5456-H117 aluminum alloy specimens included constant length parallel plate specimens measuring 1 in. x 2 in. x 1/4 in. (2.5 cm x 5.1 cm x 0.64 cm), specimens with the length varied to give a constant Reynolds number of 2×10^5 representative of laminar flow and specimens with the length varied to give a constant Reynold's Number of 10^6 representative of a transition from laminar to turbulent flow. The required lengths are shown in Table I.

TABLE I
LENGTHS REQUIRED TO MAINTAIN CONSTANT REYNOLD'S NUMBERS AS A FUNCTION OF VELOCITY

	Lengtn (Inches)	
Velocity (Knots)	Laminar Flow(1)	Transition Flow(2)
5	3.01	15.05
10	1.50	7.52
15	1.00	5.02
20	0.756	3.78
25	0.602	3.01
30	0.502	2.51
40	0.376	1.88
60	0.252	1.26

(1) Reynold's Number = 2×10^5
(2) Reynold's Number = 10^6

The specimen lengths shown in Table I were calculated from the expression for Reynold's Number for a parallel plate:

$$R_x = \frac{VL}{\nu}$$

where R_x is the Reynold's Number, V is the free stream velocity, L is the specimen length and ν is the kinematic viscosity, 1.059×10^{-5} ft/sec for sea water at 70°F. Since the kinematic viscosity

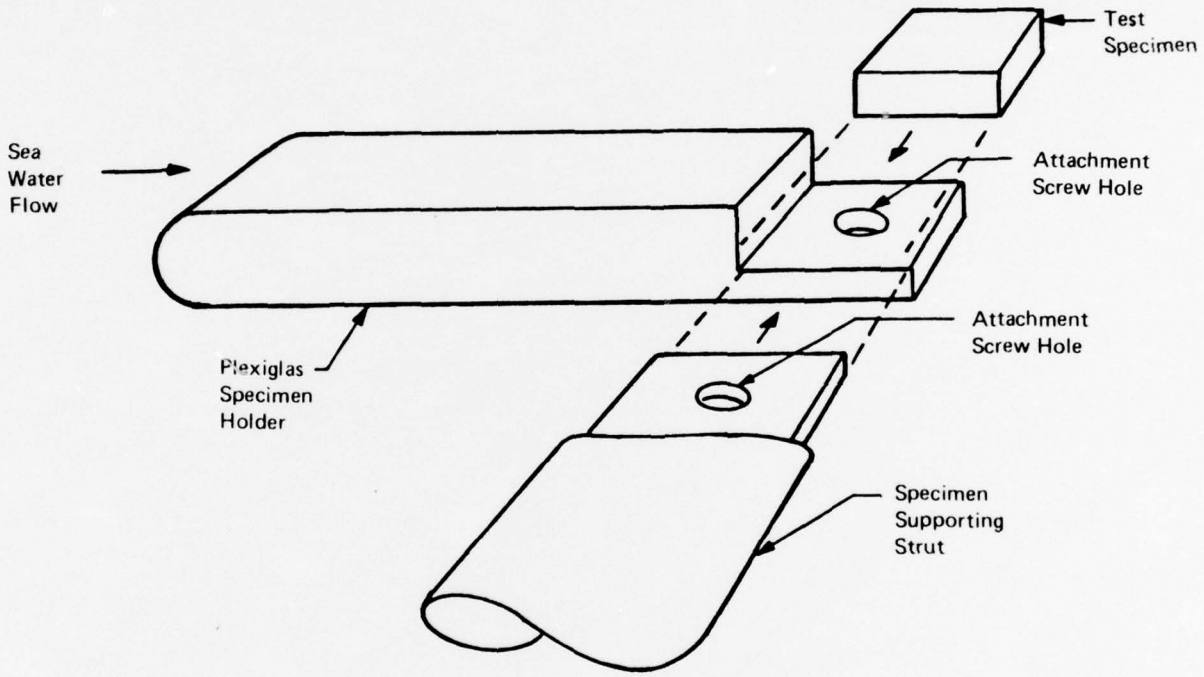

Figure 2. Schematic Representation of Specimen Holder and Specimen for Determination of Limiting Oxygen Diffusion Current Density

remains constant, the Reynold's number can be held constant by maintaining the product of velocity and length constant.

Specimens for quiescent sea water exposure had dimensions of 1 x 2 x 1/2 inches. These specimens were secured using a Stern-Makrides electrode holder for support and as an electrical contact.

RESULTS AND DISCUSSION

Cathodic Polarization - 5456-H117 Aluminum Alloy

Cathodic polarization curves were established for 5456-H117 aluminum alloy using constant length (2 inch), laminar flow and transition to turbulent flow parallel plate specimens. The effect of sea water velocity on the cathodic polarization behavior of constant length specimens is shown in Figure 3. At zero velocity, three regions were observed on the cathodic polarization curve; apparently a region where oxygen reduction is the primary cathodic process (-0.92 to -1.08 $V_{Ag/AgCl}$), a region where hydrogen reduction is the primary cathodic process (-1.08 to -1.2 $V_{Ag/AgCl}$) and a region of breakdown of water (more active than -1.2 $V_{Ag/Agcl}$). The primary cathodic process for velocities above zero velocity was the reduction of hydrogen in the potential range examined.

Cathodic polarization curves for laminar flow ($R_x = 2 \times 10^5$) specimens are shown in Figure 4. The primary cathodic process for laminar flow specimens was the reduction of hydrogen up to a potential of -1.4 $V_{Ag/AgCl}$. Breakdown of water was observed at 10 and 20 knots at potentials more active than -1.4 $V_{Ag/AgCl}$, but break down of water was not observed at 40 and 60 knots.

Cathodic polarization curves for transition to turbulent flow are shown in Figure 5. The dominant cathodic process was the reduction of hydrogen for all of the velocity ranges. Apparently, turbulent flow suppresses the breakdown of water or enhances hydrogen reduction.

Figure 6 shows the influence of velocity on the corrosion potential for constant length, laminar flow and transition to turbulent flow specimens. The corrosion potential shifted in the active direction for all flow conditions to a velocity of 10 knots, a discontinuous shift was observed in the range of 15 to 20 knots to more noble potentials, and an additional active shift was observed as the velocity was further increased. This type of behavior has previously been reported by Davis, Watts, and Gehring [1] based on anodic polarization measurements. The constant length specimens

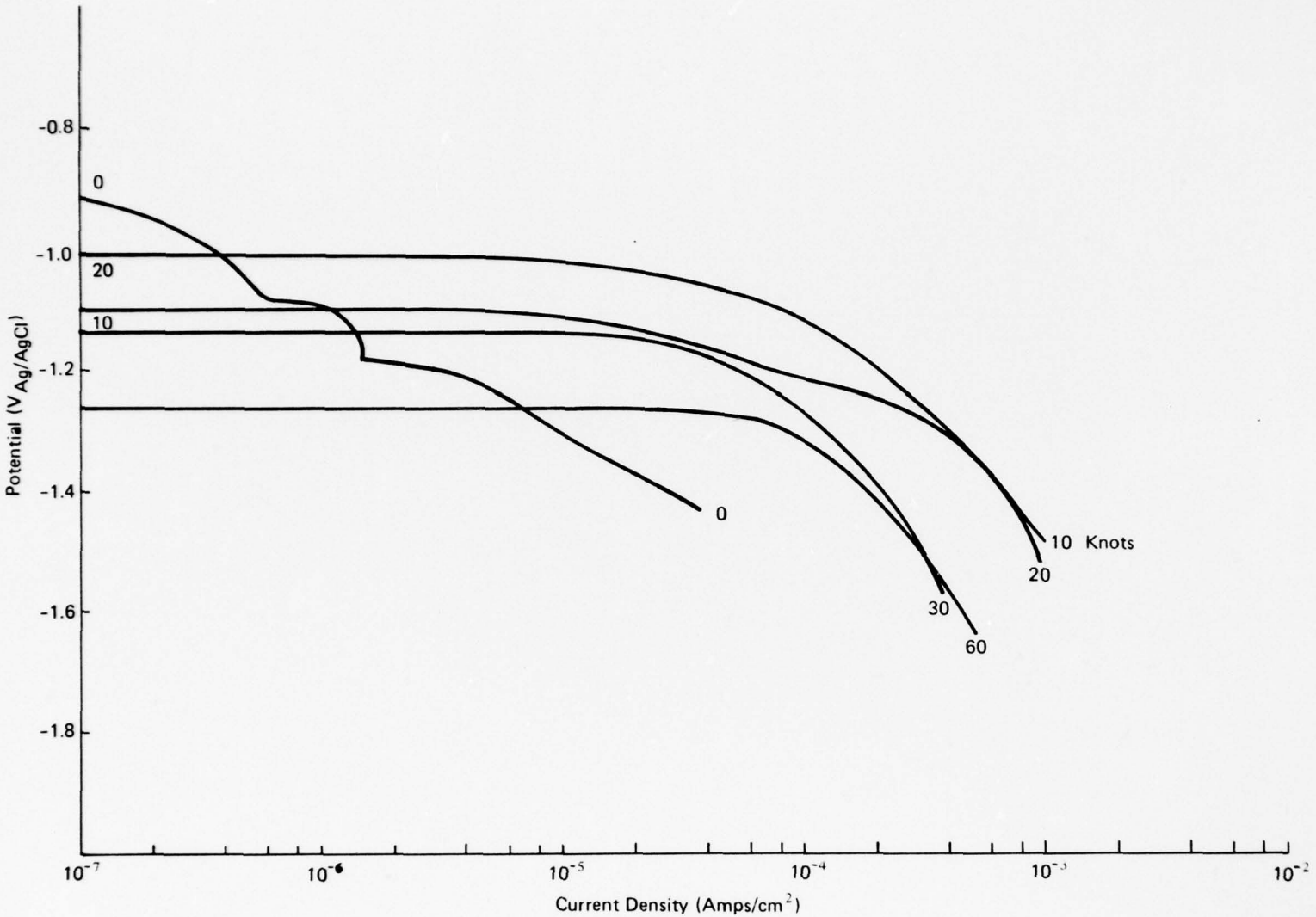

Figure 3. Effect of Sea Water Velocity on Cathodic Polarization Behavior of Constant Length Specimens

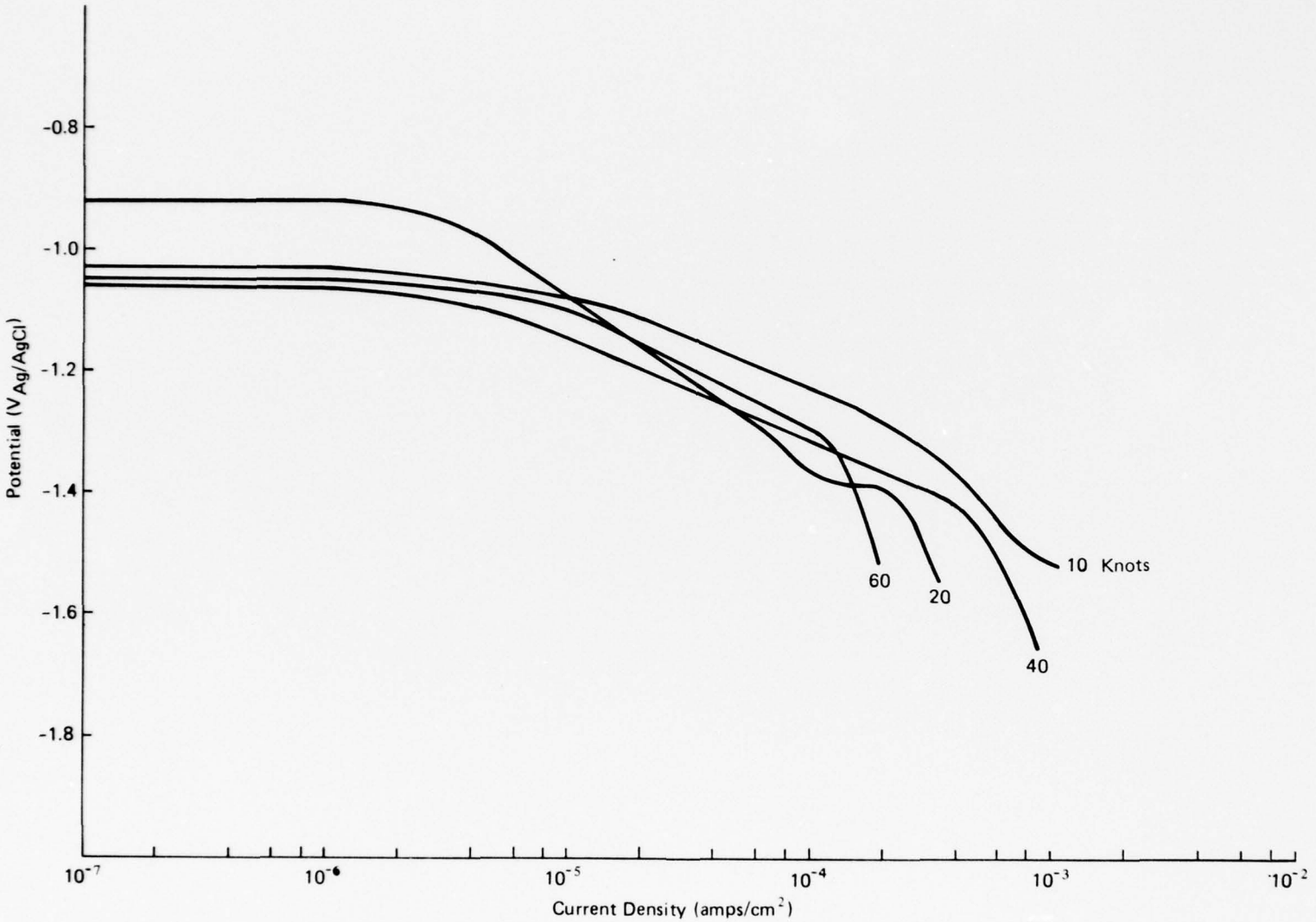

Figure 4. Effect of Sea Water Velocity on Cathodic Polarization Behavior for Laminar Flow ($R_X = 2 \times 10^5$) on 5456-H117 Aluminum Alloy

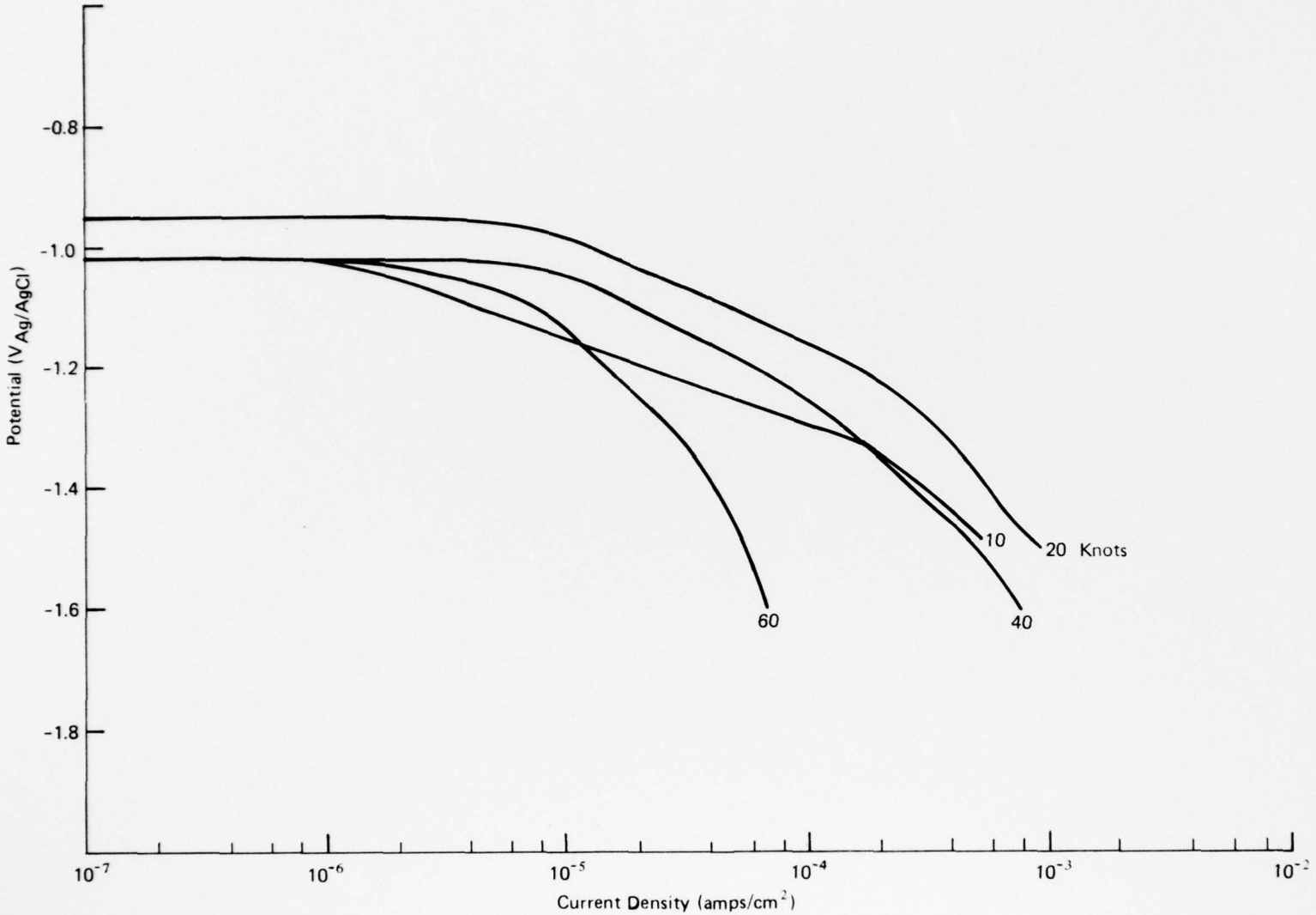

Figure 5. Effect of Sea Water Velocity on Cathodic Polarization Behavior for Transition Flow ($R_X = 10^6$) on 5456-H117 Aluminum Alloy

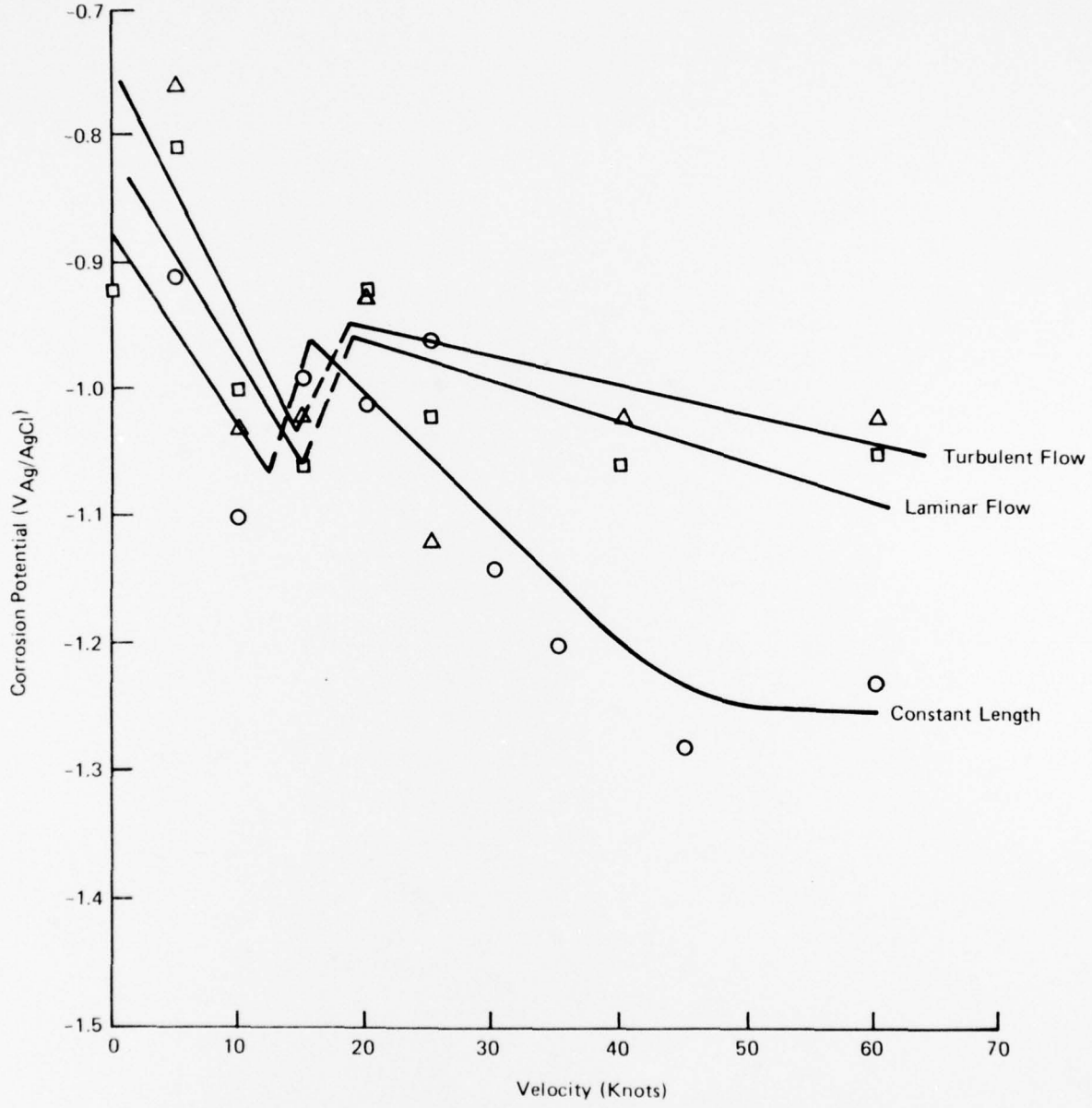

Figure 6. Effect of Velocity on the Corrosion Potential of 5456-H117 Aluminum Alloy for Constant Length, Laminar Flow, and Transition to Turbulent Flow Conditions

showed the most active potential at all velocities while the laminar flow and transition to turbulent flow specimens had essentially the same corrosion potentials as a function of velocity.

The corrosion current densities for the three flow conditions are shown in Figure 7 as a function of velocity. The corrosion current densities were determined by extrapolating the linear portion of the cathodic polarization diagram to the initial corrosion potential. The corrosion rate for constant length specimens increased by over three orders of magnitude between zero and 30 knots, but showed a decrease in corrosion rate of two orders of magnitude between 30 and 45 knots. Corrosion rate increased again from 45 to 60 knots. Similar type of behavior was previously reported by Davis and Gehring.[15] The initial increase in corrosion rate was explained by an increase in the supply of oxygen to the metal surface until sufficient oxygen was present to passivate the aluminum alloy. The corrosion rate dropped sharply after passivation but increased at higher velocities possibly due to mechanical damage to and chemical instability of the protective film.

The laminar flow and transition to turbulent flow specimens showed an increase in corrosion rate up to about 20 knots with little change in corrosion rate above 20 knots. Apparently, film instability is not as variable above 20 knots. The Reynold's Numbers for the constant length specimen are shown in Table II for comparison to Reynold's Number for variable length specimens.

TABLE II
REYNOLD'S NUMBERS AS A FUNCTION OF SEA WATER VELOCITY
FOR A TWO-INCH LENGTH SPECIMEN

Velocity (Knots)	Reynold's Number ($\times 10^{-5}$)	
0	-	
5	1.33	Laminar Flow
10	2.66	
15	3.99	
20	5.32	
25	6.65	
30	7.97	Transition to Turbulent Flow
35	9.30	
40	10.63	
45	11.96	
50	13.29	
55	14.62	
60	15.95	

Examination of the Reynold's Numbers in Table II shows that the large decrease in corrosion rate for the constant length specimen corresponds with the transition from laminar to turbulent flow

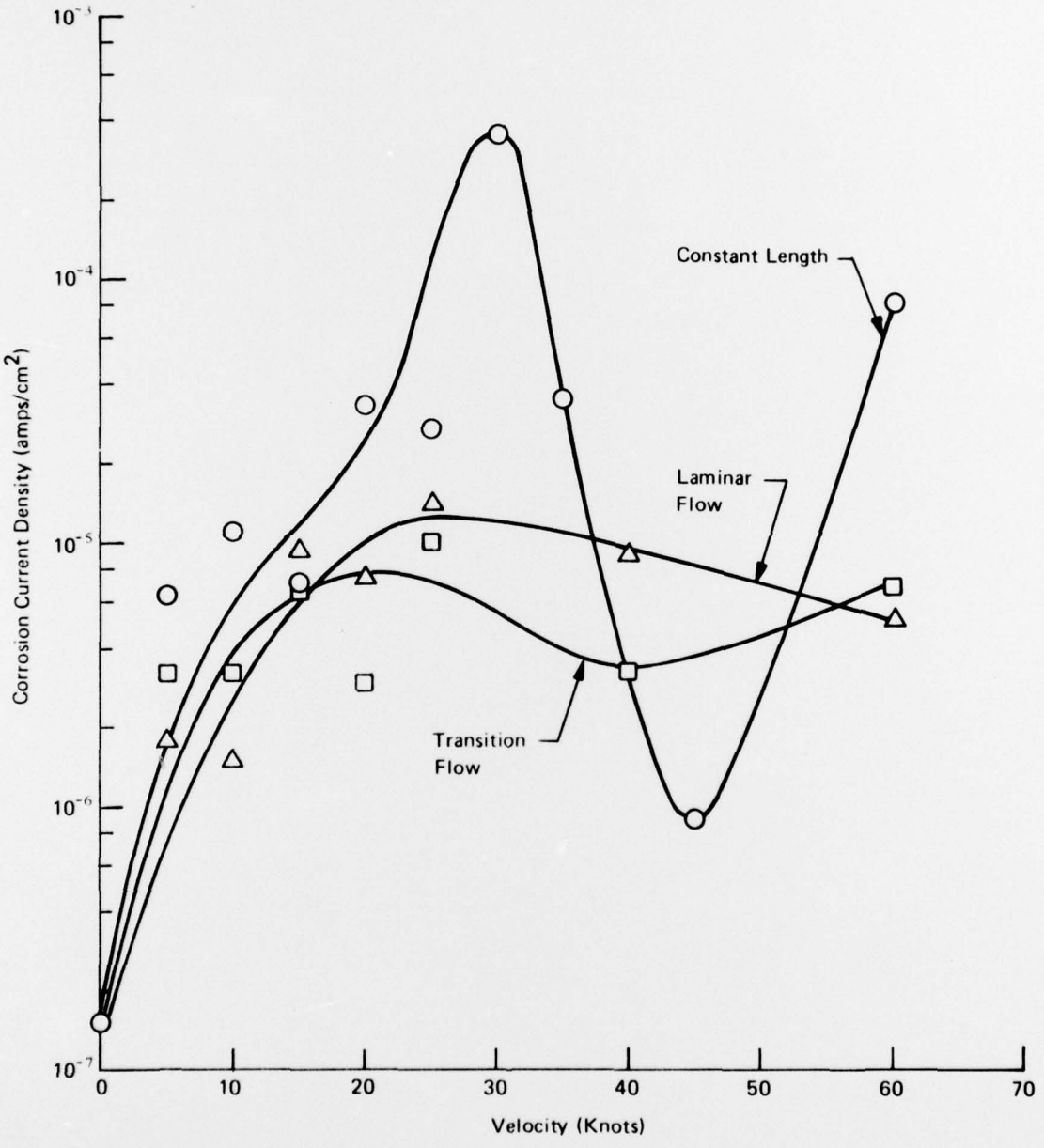

Figure 7. Effect of Velocity on Corrosion Current Densities for 5456-H117 Aluminum Alloys for Constant Length, Laminar Flow and Transition to Turbulent Flow Conditions

at 30 knots. The increase in corrosion rate at 60 knots may be explained by the higher Reynolds Number (1.6×10^6) at 60 knots compared to the laminar flow and transition to turbulent flow specimens.

Determination of Limiting Oxygen Diffusion Current Density

The corrosion rate and corrosion potential of aluminum exposed to low velocity sea water are proposed to be controlled by the magnitude of the limiting oxygen diffusion current density. The limiting oxygen diffusion current density is given by the expression:

$$i_L = \frac{DnFC_B}{\delta_m}$$

Where i_L is the limiting oxygen diffusion current density, D is the diffusion coefficient for oxygen, n is the number of electrons transferred, F is Faraday's constant, C_B is the bulk solution concentration of oxygen and δ_m is the mass transport boundary layer thickness. Three hydrodynamic parameters are important in establishing the mass transfer effects on corrosion as a function of sea water velocity. The Reynold's Number describes the hydrodynamic boundary layer thickness as a function of velocity. The Reynold's Number for a parallel plate is given by the expression:

$$R_x = \frac{VL}{\nu}$$

where V is the free stream velocity, L is the length and ν is the kinematic viscosity. The hydrodynamic boundary layer thickness is given by the expression:

$$\delta_h = L(30/R_x)^{0.5}$$

for laminar flow conditions and:

$$\delta_h = L\frac{0.38}{R_x^{0.2}}$$

for turbulent flow conditions. The mass transfer boundary layer thickness is related to the hydrodynamic boundary layer thickness by the expression:

$$\delta_m = \frac{\delta_h}{Sc^{1/3}}$$

where Sc is the Schmidt Number given by the expression:

$$Sc = \frac{\nu}{D}$$

The limiting oxygen diffusion current density can be expressed in terms of the Reynold's and Schmidt Numbers according to the expressions:

$$i_L = \frac{DnFC_B Sc^{1/3}}{L\sqrt{30/R_x}} \text{ for laminar flow}$$

and

$$i_L = \frac{DnFC_B Sc^{1/3}}{L(0.38/R_x^{0.2})} \text{ for turbulent flow}$$

Substituting the appropriate variables for the Reynold's and Schmidt Numbers gives the velocity dependence of the limiting oxygen diffusion current density:

$$i_L = \frac{D^{0.67}\, nFC_B\, V^{0.5}}{5.48\, L^{0.5}\, \nu^{0.17}}$$

for laminar flow and

$$i_L = \frac{D^{0.67}\, nFC_B\, \nu^{0.12}\, V^{0.2}}{0.38\, L^{0.8}}$$

for turbulent flow conditions.

If all the variables are maintained constant except for the velocity, the limiting oxygen diffusion current density is proportional to velocity as follows:

$$i_L \propto V^{0.5} \quad \text{for laminar flow}$$

$$i_L \propto V^{0.2} \quad \text{for turbulent flow}$$

Typical cathodic polarization curves on constant length platinum clad tantalum specimens are shown in Figure 8. The limiting oxygen diffusion current density increased by over two orders of magnitude when the velocity was increased from zero to ten knots. Further increases in velocity have little influence on the limiting oxygen diffusion current density.

The limiting oxygen diffusion current as a function of sea water velocity is shown in Figure 9. A logarithmic relationship was not observed between limiting oxygen diffusion current density and velocity as predicted. The limiting oxygen diffusion current density was essentially independent of velocity above 15 knots. A complete explanation for the independence of limiting oxygen diffusion current density with increasing velocity will require additional work.

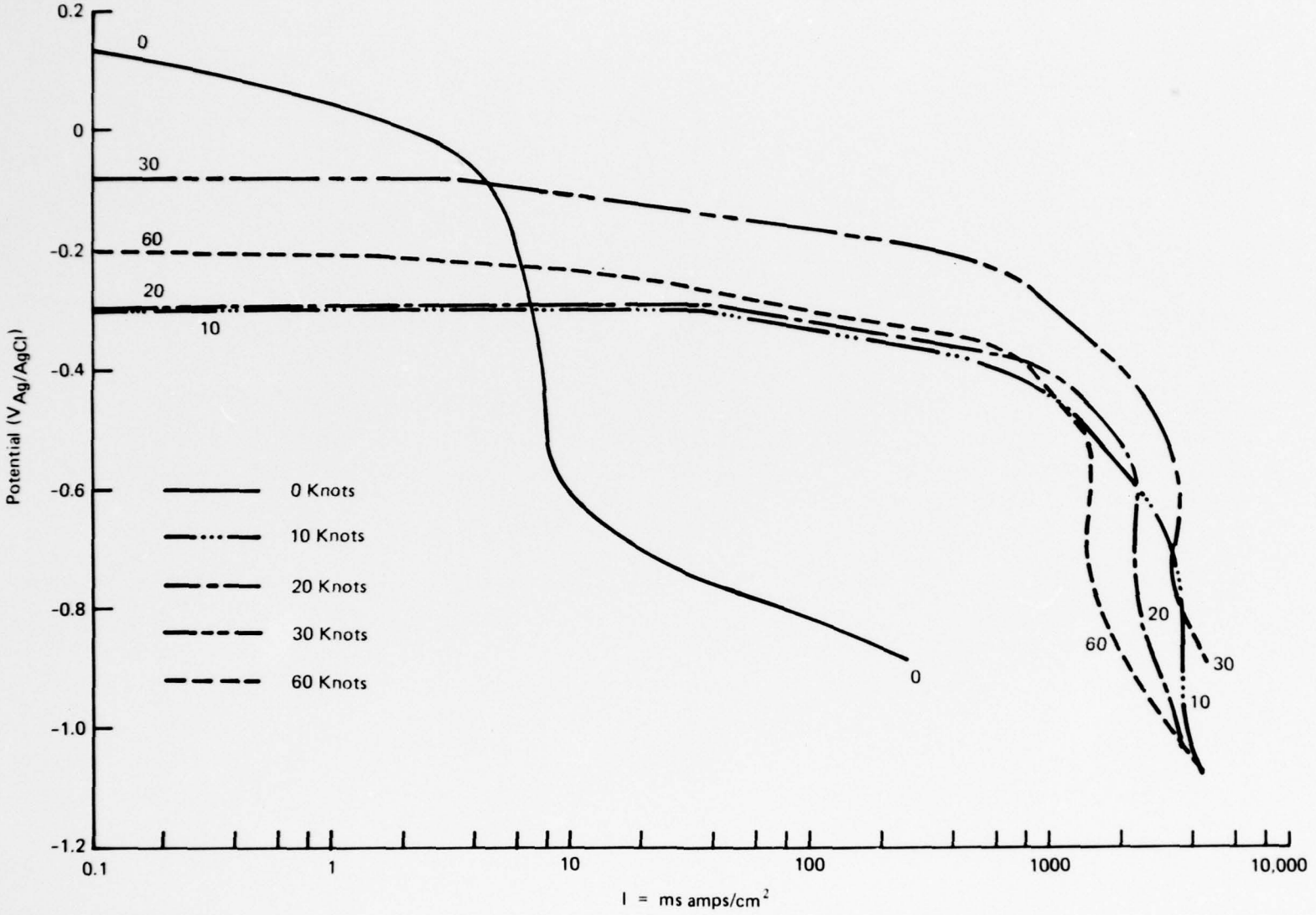

Figure 8. Carpet Plot of Cathodic Polarization Curves for Pt-Clad Tantalum

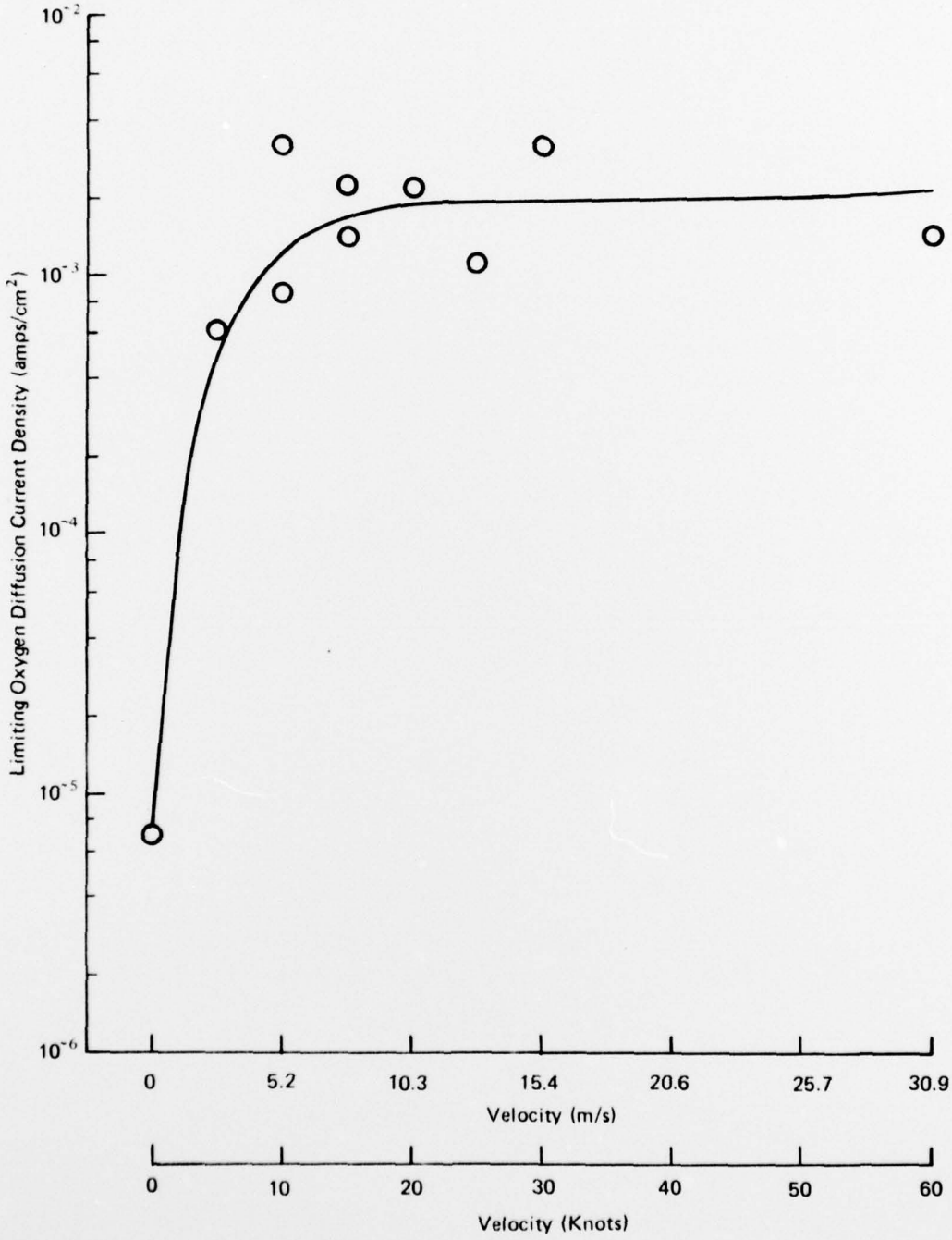

Figure 9. Limiting Oxygen Diffusion Current Density as a Function of Sea Water Velocity

Surface Characteristics of Constant Potential Test Specimens

Surfaces of a few specimens were examined that were exposed to sea water at 15, 30 and 60 knots with an applied potential of -1.0 $V_{Ag/AgCl}$ for 24 hours. Optical micrographs and scanning electron micrographs are shown in Figure 10 for 15 knots, Figure 11 for 30 knots and Figure 12 for 60 knots. At 15 knots, pits are observed with the optical micrograph (Figure 10a) as dark spots on a light surface. A scanning electron micrograph (Figure 10b) shows a non-uniform scale with many apparent fractures. At 30 knots, less cracking and spalling of the film was observed (Figure 11a). Examination of the latter surface with the scanning electron microscope (Figure 11b) shows that the surface oxide is much more uniform than was observed at 15 knots. Furthermore, there were fewer cracks in the film at 30 knots than observed at 15 knots.

The surface at 60 knots looked very similar optically to the surface at 15 knots (Figure 12a). However, a scanning electron micrograph shows much more cracking and spalling at 60 knots than at 15 knots. Hence, based on these limited results the oxide film appears to become more uniform as the velocity increases with some cracking at 15 knots, less cracking at 30 knots, and extensive cracking and spalling at 60 knots. Additional studies are desirable on metallurgically polished surfaces to investigate the effects of velocity and applied potential on surface morphology and resultant corrosion behavior.

Preferential corrosion was observed around non-metallic inclusions at all of the velocities. Figure 13 shows this preferential attack at the interface between a non-metallic inclusion after 24 hours exposure to 30 knot sea water. Figure 14 shows similar preferential corrosion at the matrix-intermetallic inclusion interface after 24 hours exposure to 60 knot sea water at an applied potential of -1.0 $V_{Ag/AgCl}$.

It appears that increasing velocity and the application of applied potentials changes the basic nature of the film on 5456-H117 aluminum alloy. Pitting appears to be initiated at non-metallic inclusions where the integrity of the film is not as great as in areas not containing non-metallic inclusions. Local galvanic action reduces the chemical stability of the film markedly. The pitting that was observed at an applied potential of -1.0 $V_{Ag/AgCl}$ occurred at a potential more active than the pitting potential and the protection potential and is not predicted on the basis of current pitting theory. The pitting observed at -1.0 $V_{Ag/AgCl}$ was not as extensive as pitting observed at the same velocities at applied potential levels more noble than the critical pitting potential.[1] It is possible that non-

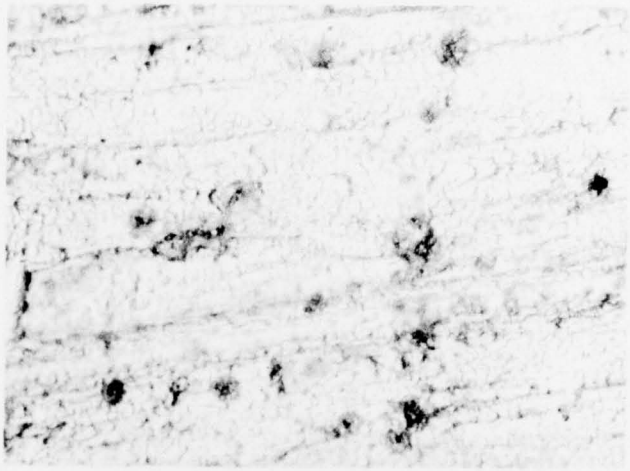

a. Optical 450X

b. Scanning Electron Micrograph 1950X

Figure 10. Pitting Behavior and Scale Microstructure
(15 Knots: - 1.0 $V_{Ag/Ag\,Cl}$)

a. Optical 450X

b. Scanning Electron Micrograph 1950X

Figure 11. Pitting Behavior and Scale Microstructure
(30 Knots: - 1.0 $V_{Ag/Ag\ Cl}$)

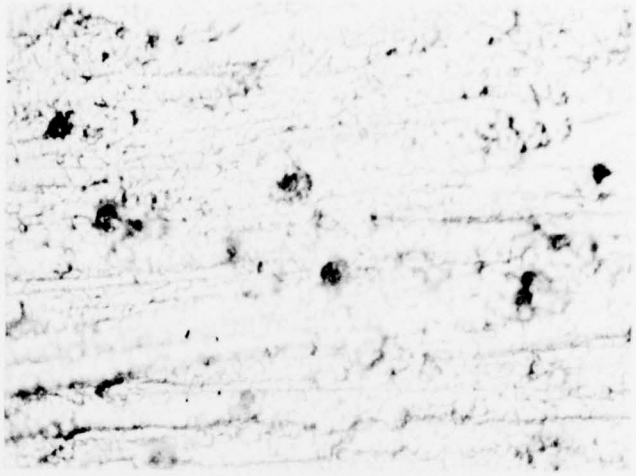

a. Optical 450X

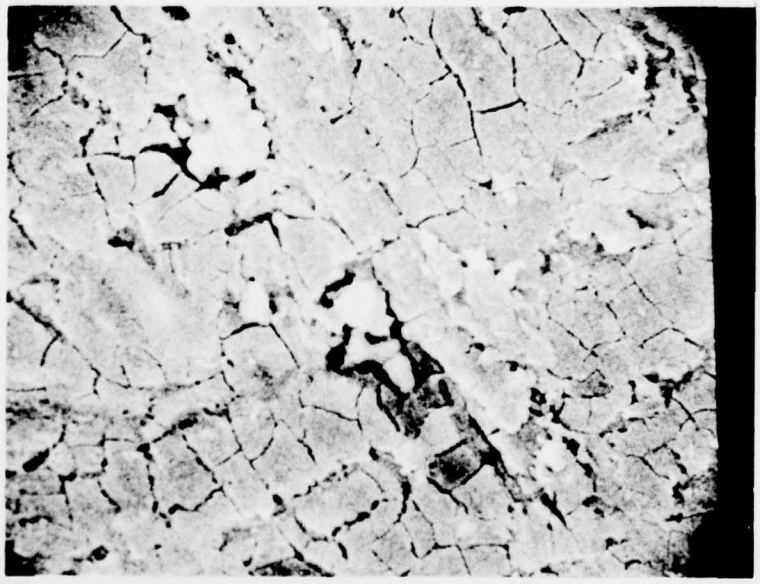

b. Scanning Electron Micrograph 1950X

Figure 12. Pitting Behavior and Scale Microstructure
(60 Knots: - 1.0 $V_{Ag/Ag\ Cl}$)

Scanning Electron Micrograph 2950X

Figure 13. Pitting at Inclusions (30 Knots: - 1.0 $V_{Ag/Ag\ Cl}$)

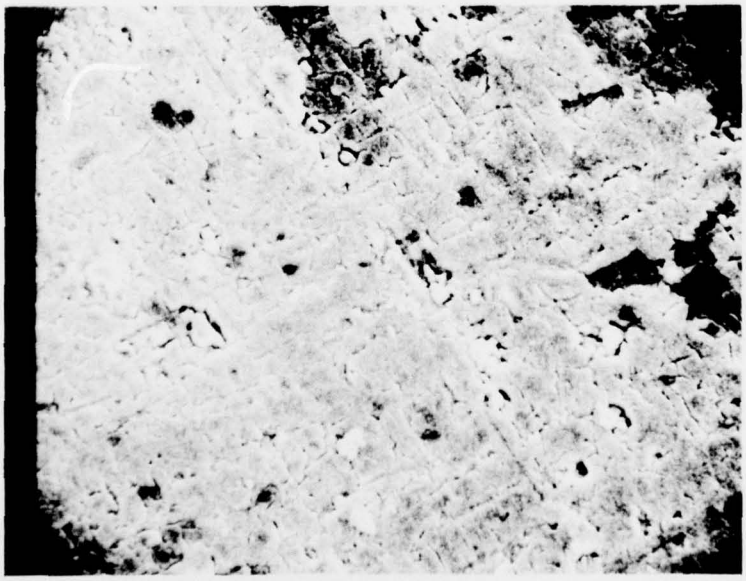

Scanning Electron Micrograph 650X

Figure 14. Pitting at Inclusions (60 Knots: - 1.0 $V_{A/gAg\ Cl}$)

metallic inclusions may not be required to initiate pitting at potentials more noble than the critical pitting potential, but non-metallic inclusions may be required to initiate pitting at potentials more active than the protection potential. It can be postulated that film stability is a complex function of applied potential, sea water velocity, boundary layer variables, and the thermodynamic chemical potential of the film.

SUMMARY AND CONCLUSIONS

1. Cathodic polarization studies on 5456-H117 aluminum alloy in flowing sea water indicate that the primary cathodic process at zero velocity is oxygen reduction and at velocities above 10 knots is hydrogen reduction.
2. Determination of the limiting oxygen diffusion current density as a function of velocity has shown that the limiting oxygen diffusion rate increased by several orders of magnitude up to 10 knots and is independent of velocity from 10 knots to 60 knots.
3. Increasing velocity resulted in a more uniform oxide film when going from 15 knots to 30 knots to 60 knots at an applied potential level of -1.0 $V_{Ag/AgCl}$. Fissures were observed after 24 hours exposure at 15 knots. Exposure at 30 knots showed fewer fissures while exposure at 60 knots showed extensive fissures and some spalling of the film. Pits formed at all of the velocities could be associated in many cases with non-metallic inclusions.
4. A mechanism is suggested for the influence of applied potential on the pitting behavior of 5456-H117 aluminum alloy as a function of applied potential. At applied potentials more noble than the critical pitting potential, pits initiate at random. At potentials more active than the protection potential, pits are initiated at the interface between the matrix and non-metallic inclusions.

ACKNOWLEDGEMENTS

This research was funded by the Office of Naval Research Department of Materials Science under Contract No. N00014-75C-1087. The authors wish to acknowledge the guidance provided by Dr. P.A. Clarkin of that office.

REFERENCES

1. J.A. Davis, A.A. Watts, and G.A. Gehring, Jr., "Pitting Behavior of Aluminum Alloys in High Velocity Sea Water," paper presented at the Annual Conference of the Electrochemical Society, October 18-22, 1976, Las Vegas, Nevada.
2. M. J. Pryor, Proceedings of the International Conference on Localized Corrosion, R. W. Staehle, B. F. Brown, J. Kruger, and A. Agrawal, Editors, NACE (1974), p. 2.
3. J. R. Galvele, S. M. DeMicheli, I. L. Mueller, S. B. deWexler, and I. L. Alanis, Proceedings of the International Conference on Localized Corrosion, R. W. Staehle, B. F. Brown, J. Kruger and A. Agrawal, Editors, NACE (1974), p. 580.
4. G. C. Wood, W. H. Sutton, J. A. Richardson, T. N. K. Riley, and A. G. Malherbe, Proceedings of the International Conference on Localized Corrosion, R. W. Staehle, B. F. Brown, J. Kruger and A. Agrawal, Editors, NACE (1974) p. 526.
5. W. H. Hartt, presented at Corrosion/74, Paper No. 80, March 4-8, 1974, Chicago, Illinois.
6. R. E. Groover, T. J. Lennox and M. H. Peterson, Materials Protection, 8 (1969) p. 25.
7. W. H. Ailor, presented at NACE 26th Annual Conference, March 2-6, 1970, Philadelphia, Pa.
8. F. W. Fink and W. K. Boyd, The Corrosion of Metals in Marine Environments, Bayer and Company, Inc. (1970).
9. F. Franz and P. Novak, Proceedings of the International Conference of Localized Corrosion, R. W. Staehle, B. F. Brown, J. Kruger, and A. Agrawal, Editors, NACE (1974) p. 576.
10. G. J. Danek, Naval Engineers Journal, (October 1966), p. 763.
11. Barry C. Syrett, "Erosion-Corrosion of Copper-Nickel Alloys in Seawater and other Aqueous Environments", Corrosion, 32, (1976) p. 242.
12. Theodore R. Beck, Paper No. 77 presented at Corrosion/76, March 22-26, 1976, Houston, Texas.
13. Aladar Tvarusko, J. Electrochem. Soc., Vol. 123, (1976) p. 489.
14. F. Mansfeld and J. V. Kenkel, Paper No. 100 presented at Corrosion/77, (March 14-18, 1977), San Francisco, California.
15. J. A. Davis and G. A. Gehring, Jr., Materials Performance, 13, (1975) p. 32.